Fusion cross section behavior for $^{12}C + ^{24}Mg$ and $^{12}C + ^{26}Mg$

K. Daneshvar* and D. G. Kovar
Argonne National Laboratory, Argonne, Illinois 60439

S. J. Krieger
University of California, Lawrence Livermore National Laboratory, Livermore, California 94550

K. T. R. Davies
Oak Ridge National Laboratory, Oak Ridge, Tennessee 37830

(Received 18 June 1981)

Total fusion cross section excitation functions for the $^{12}C + ^{24}Mg$ and $^{12}C + ^{26}Mg$ systems have been measured in the energy range $20 \leq E_{lab} < 60$ MeV by detection of the evaporation residues. The excitation function for $^{12}C + ^{24}Mg$ is found to show evidence of oscillatory structures with peak to valley difference of $\sim 5-10\%$ while that for $^{12}C + ^{26}Mg$ is relatively smooth. The maximum fusion cross section for $^{12}C + ^{24}Mg$ is observed to be ~ 1180 mb compared to ~ 1280 mb for $^{12}C + ^{26}Mg$. The cross sections for $^{12}C + ^{26}Mg$ show evidence of a change in behavior at a bombarding energy significantly below the energy at which the cross section saturates. The results are discussed in the context of previous measurements and predictions of macroscopic and microscopic fusion models.

[NUCLEAR REACTIONS Fusion measurement, $\sigma_{fus}(E)$: $^{12}C + ^{24}Mg$, $20 \leq E_{lab} \leq 63$ MeV; $^{12}C + ^{26}Mg$, $20 \leq E_{lab} \leq 56$ MeV; measured $\sigma_{elastic}(\theta)$, $\sigma_{fusion}(\theta)$ at $E_{lab} = 20$, 24, 30, 41, 48, 56, and 60 MeV for $^{12}C + ^{24}Mg$, and at 20, 30, 42, and 56 MeV for $^{12}C + ^{26}Mg$.]

I. INTRODUCTION

Over the last few years significant experimental and theoretical attention has been focused on the question of what role the detailed properties of the nuclei involved play in the fusion process. Obervations of resonancelike structures in the total fusion cross section excitation function, $\sigma_{fus}(E)$,[1-4] and variations in the maximum fusion cross section, σ_{fus}^{max},[1,3-5] for light-heavy-ion systems ($10 \leq A_{proj,targ} \leq 18$) have been interpreted as indications of such dependences. Particularly striking is the observation that the resonance structures appear prominently, as $10-20\%$ deviations from the average behavior, in systems involving "α nuclei" (i.e., $^{12}C + ^{12}C$, $^{12}C + ^{16}O$, and $^{16}O + ^{16}O$), but are relatively damped or completely absent in neighboring systems. The exception to this are systems involving ^{14}C where strong structures have recently been observed in several exit channels.[6] These gross structures have almost regular spacings of $\sim 3-5$ MeV in the center of mass system and are found to be primarily present in the α-evaporating channels which are associated with high spin states in the compound nucleus and with large partial waves in the entrance channel.

One has generally interpreted the gross structures to be associated with shape resonances produced in the surface transparent potential required to fit the elastic scattering. This type of potential reflects the availability of only a few reaction channels for the incoming grazing partial waves. As one goes to heavier systems one might expect the condition to no longer be fulfilled and the potential describing the entrance channel to be strongly absorbing. However, recent studies have shown that the elastic and inelastic scattering for ^{12}C and ^{16}O projectiles on heavier "α-nucleus" targets (e.g., ^{24}Mg, ^{28}Si, and ^{32}S) display unexpectedly large strengths at back angles.[7,8] This could be interpreted as evidence for a much more surface transparent potential than had been believed. Furthermore, the excitation functions for the elastic and inelastic scattering cross sections at 180° show prominent resonancelike

structures very reminiscent of that observed for the lighter systems. These behaviors are not understood at present and information regarding other exit channels, in particular the fusion channel, would be of great interest in helping to reveal the nature of these phenomena.

While a number of fusion cross section measurements have been reported for systems involving ^{12}C and ^{16}O projectiles on target nuclei within the *sd* shell,[3,9] the focus of the investigations has not in general been on the question of whether structure is present in the excitation function. Evidence for possible structure has been reported for $^{12}C + ^{20}Ne$,[10] $^{12}C + ^{24}Mg$,[11] and $^{12}C + ^{28}Si$,[12] while negative results are reported for all systems involving ^{16}O.[11–14] The present paper reports the results of total fusion cross section measurements for the $^{12}C + ^{24}Mg$ and $^{12}C + ^{26}Mg$ systems. While the primary motivation was to establish whether resonancelike structures exist in the excitation functions, the study of the two Mg isotopes also allows investigation of whether significant differences are present in the average cross section behaviors indicative of a target-projectile dependence.

The experimental technique and results will be presented in Secs. II and III, respectively. The comparison with other experimental results accumulated on similar mass systems and the prediction of theoretical models will be discussed in Sec. IV. In Sec. V, a summary and conclusion will be given.

II. EXPERIMENTAL DETAILS

The experiments were performed using ^{12}C beams from the Argonne National Laboratory FN tandem accelerator. The experimental setup and techniques used were similar to those used in previous studies.[3] The beams were tightly collimated at the entrance to the 178 c.m. scattering chamber in which the fusion measurements were performed, and monitored by two silicon detectors placed at $\pm 11°$ of the beam axis. In the scattering chamber a third similar detector was used for measuring the elastic scattering at relatively back angles and served as an alternative means of normalizing the fusion yields. The absolute angle of the fusion detector was established by measuring the elastic scattering on either side of the beam direction ($\pm 6°$) and is believed to be determined to $\pm 0.05°$. An electropolished tantalum slit of 0.8 mm diameter was used to define the solid angle of the fusion detector (located at distances $25 \leq d \leq 50$ cm).

The ^{24}Mg and ^{26}Mg targets were isotopically enriched (99.4% and 95.6% respectively) self-supporting foils of thickness 75–125 $\mu g/cm^2$. The targets were stored and transferred under vacuum to minimize oxidation. During the measurements a liquid nitrogen-cooled shroud surrounded the target to prevent carbon buildup. The fusion cross sections were established by measurement of the evaporation residues using a ΔE-E gas ionization counter-silicon detector system similar to that of Fowler and Jared.[15] An example of the spectrum obtained for the $^{12}C + ^{24}Mg$ reaction is shown in Fig. 1. The yields at large ΔE can clearly be identified as evaporation residues, although, as can be seen, the yields of the various Z's are not separated. A portion of the tail extending to lower ΔE was identified to be evaporation residues based on the shape of the energy spectrum. The integrated yields in this region were not more than $\sim 2-3\%$ of that in the main body of yield at large ΔE.

III. RESULTS AND ANALYSIS

A. Elastic scattering

As can be observed in Fig. 1, the fusion detector allowed simultaneous measurement of elastic scattering and evaporation residues. The elastic scattering angular distributions were established at the forward angles (i.e., $\theta_{lab} = 3°-25°$) using the ΔE-E detector, and at larger angles using a silicon detector with somewhat larger solid angle. Examples of the elastic scattering angular distributions measured are shown in Figs. 2 and 3. The dashed lines in these figures are the results of a simultaneous fit of the elastic scattering angular distribution at all energies using the code PTOLEMY.[16] The

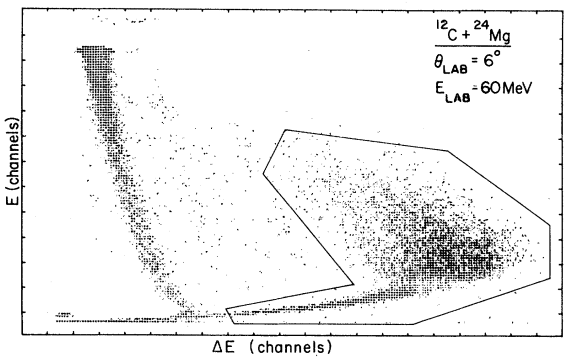

FIG. 1. The ΔE vs E spectrum for the $^{12}C + ^{24}Mg$ reaction at $E_{lab} = 60$ MeV and $\theta_{lab} = 6°$.

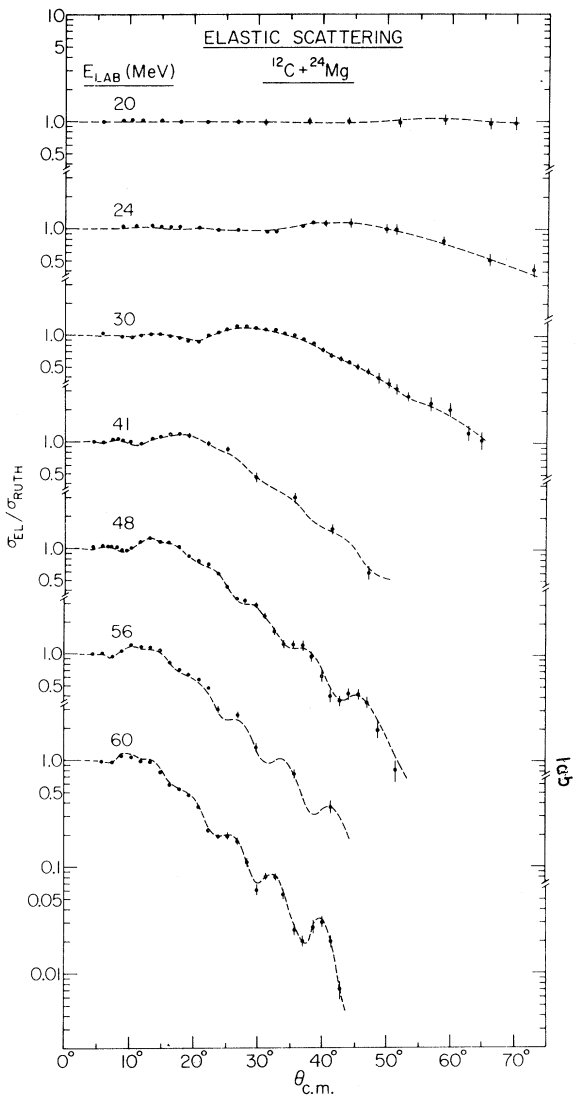

FIG. 2. Elastic scattering angular distributions measured for $^{12}C + ^{24}Mg$. The dashed curves represent optical model calculations obtained from the energy independent potential described in Table I.

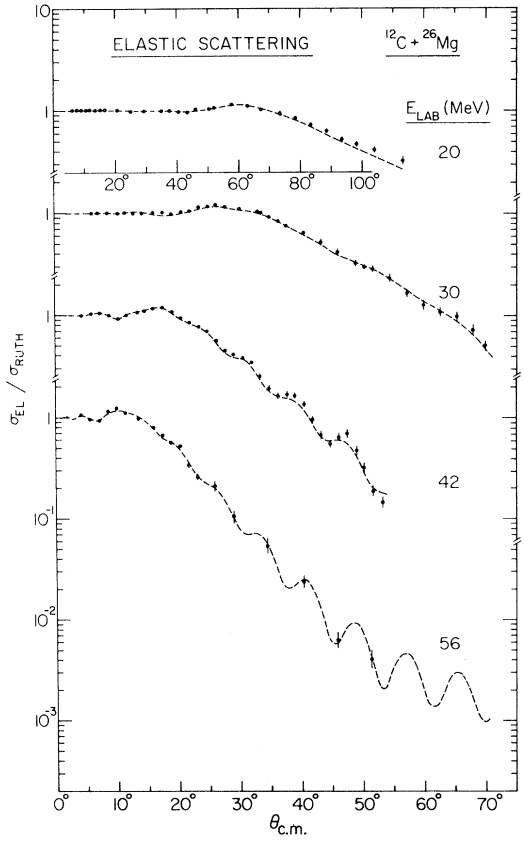

FIG. 3. Elastic scattering angular distributions measured for $^{12}C + ^{26}Mg$. The dashed curves represent optical model calculations obtained from the energy independent potential described in Table II.

analysis was performed to establish the total reaction cross sections and for use in normalizing the fusion data. Individual fits at each energy were also performed in which it was found that, while somewhat better fits could be obtained, the total reaction cross sections were in agreement with that found in the simultaneous fit of the data at all energies. The results of the fits for $^{12}C + ^{24}Mg$ and $^{12}C + ^{26}Mg$ are summarized in Tables I and II, respectively.

B. Fusion cross sections

Angular distributions for the fusion products were measured in the angular range $3° \leq \theta_{lab} \leq 35°$. Typical angular distributions obtained for $^{12}C + ^{24}Mg$ and $^{12}C + ^{26}Mg$ are shown in Figs. 4 and 5. As can be seen, these angular distributions are forward peaked and approximately fall exponentially as function of angle. The shapes of the angular distributions at forward angles vary slowly with energy. The change in slope at back angles is mainly due to evaporation of alpha particles which particularly affect the distribution at the lowest bombarding energy.

The absolute normalization of the fusion cross sections was established at small angles where the elastic scattering is Rutherford. Optical model fits to elastic data were used to facilitate this procedure. This method of normalization is very good at low energies and is estimated to contribute no more than

TABLE I. Optical model parameters for $^{12}C + ^{24}Mg$. Fit *A* is a simultaneous fit to all elastic angular distributions using an energy independent potential. Fit *B* is an individual fit at each energy. The optical potential is given by the following expressions,

$$V(R)=V^c(r)-Vf(r)-iWg(r),$$

$$V^c(r)=\begin{cases}\dfrac{Z_1Z_2e^2}{r}, & r>R_c,\ R_c=r_{\phi c}(A_1^{1/3}+A_2^{1/3}),\\ \dfrac{Z_1Z_2e^2}{2R_c(3-r^2/R_c^2)}, & r<R_c\end{cases},$$

$$f(r)=\{1+\exp[(r-R)/a]\}^{-1},\quad R=r_0(A_1{}^{1/3}+A_2{}^{1/3}),$$

$$g(r)=\{1+\exp[(r-R_I)/a_I]\}^{-1},\quad R_I=r_{0I}(A_1{}^{1/3}+A_2{}^{1/3}).$$

E_{lab} (MeV)	V (MeV)	r_0 (fm)	a (fm)	W (MeV)	r_{0I} (fm)	a_I (fm)	$r_{\phi c}$ (fm)	χ^2	σ_{react} (mb)	Fit
20.0	16.10	1.37	0.48	85.6	1.19	0.40	1.25	1.84	334	*A*
										B[a]
24.0	16.10	1.37	0.48	85.6	1.19	0.40	1.25	3.96	641	*A*
										B[a]
30.0	16.10	1.37	0.48	85.6	1.19	0.40	1.25	3.57	938	*A*
	16.99	1.34	0.46	6.8	1.22	0.34	1.25	2.41	881	*B*
41.0	16.10	1.37	0.48	85.6	1.19	0.40	1.25	6.35	1232	*A*
	11.83	1.33	0.45	58.5	1.18	0.31	1.25	3.82	1225	*B*
48.0	16.10	1.37	0.48	85.6	1.19	0.40	1.25	8.02	1340	*A*
	16.18	1.50	0.31	230.9	1.37	0.15	1.25	2.23	1308	*B*
56.0	16.10	1.37	0.48	85.6	1.19	0.40	1.25	8.50	1425	*A*
	6.53	1.51	0.40	207.1	1.14	0.38	1.25	2.97	1423	*B*
60.0	16.10	1.37	0.48	85.6	1.19	0.40	1.25	6.87	1458	*A*
	16.89	1.34	0.54	28.6	1.29	0.53	1.25	6.55	1521	*B*

[a]Data insufficient to obtain meaningful parameters.

TABLE II. Optical model parameters for $^{12}C + ^{26}Mg$. See Table I for explanation of parameters.

E_{lab} (MeV)	V (MeV)	r_0 (fm)	a (fm)	W (MeV)	r_{0I} (fm)	a_I (fm)	$r_{\phi c}$ (fm)	χ^2	σ_{react} (mb)	Fit
20.0	10.0	1.32	0.64	20.0	1.24	0.50	1.25	5.10	506	*A*
										B[a]
30.0	10.0	1.32	0.64	20.0	1.24	0.50	1.25	3.78	982	*A*
	19.2	1.42	0.40	86.46	1.35	0.21	1.25	2.63	1002	*B*
42.0	10.0	1.32	0.64	20.0	1.24	0.50	1.25	2.41	1309	*A*
	21.7	1.46	0.30	36.62	1.43	0.20	1.25	1.34	1338	*B*
56.0	10.0	1.32	0.64	20.0	1.24	0.50	1.25	4.30	1452	*A*
	15.1	1.26	0.67	27.00	1.20	0.50	1.25	3.28	1492	*B*

[a]Data insufficient to obtain meaningful parameters.

$\approx 3\%$ uncertainty at higher energies. The total fusion cross section was established by integrating the differential cross section angular distribution. To do so, smooth extrapolations were made into angular regions not measured because of experimental difficulties. Extrapolations into the angular regions $\theta_{lab} < 3°$ and $\theta_{lab} > 35°$ are shown in Figs. 4 and 5. This procedure is estimated to contribute no more than $\approx 2\%$ uncertainty to the absolute cross section. Tables III and IV summarize the results determined from the fusion angular distribution measurements.

The excitation function for evaporation residues was measured in much finer energy steps at a fixed angle near the maximum in $(\delta\sigma/\delta\Omega) * \sin\theta$. This corresponds to $\sim 8°$ in the laboratory system over the entire energy range studied, as can be seen in Figs. 4 and 5. The differential cross sections were obtained from the yields using the beam current integrator. Normalization using the elastic scattering yields in the monitor gave results in agreement with that obtained using the integrator. The $\sigma_{fus}(E)$ was obtained from the single angle measurements by establishing the ratio of the total fusion cross section to the differential cross section, $(d\sigma/d\Omega\ (\theta_{lab}=8°))$, at those energies where the angular distributions were measured. This ratio was found to have a linear behavior as function of energy and provided the factor for obtaining the total fusion cross section from the single angle yield. This procedure is estimated to contribute $\lesssim 2\%$ to the uncertainty in the absolute cross section.

In Fig. 6 the $\sigma_{fus}(E)$ obtained for the $^{12}C + ^{24}Mg$ and $^{12}C + ^{26}Mg$ systems are shown plotted versus $E_{c.m.}$. The solid lines represent the total reaction cross section determined from the optical model fits to the elastic scattering. The solid data points represent the fusion cross sections obtained from the single angle measurements and the open circles represent those obtained from the angular distribution measurements. The circles shown in Fig. 6 indicate the relative uncertainties which are $\sim 2-3\%$. The absolute errors on the total fusion cross sections (which are of the order of $6-7\%$) are shown in Figs. 7 and 8, where total fusion is plotted as a function of $1/E_{c.m.}$. Since the energy lost in the target was small, the energy values used here are those of the beam at the front of target (i.e., the energies at the center of target are estimated to be ~ 100 and 25 keV smaller at the lowest and highest bombarding energies, respectively).

IV. DISCUSSION

A. Oscillatory behavior in $\sigma_{fus}(E)$

The excitation function for $^{12}C + ^{24}Mg$ is observed to display structures with peak-to-valley variation of $50-100$ mb (i.e., $5-10\%$), while that for $^{12}C + ^{26}Mg$ is found to behave rather smoothly. Because of the small magnitude of the effects, a number of checks were made to ensure the structures were real. Among these were the use of different normalization procedures and repetition of measurement using different targets. Perhaps most convincing were the consecutive measurements of $^{12}C + ^{24}Mg$ and $^{12}C + ^{26}Mg$ reactions using the same experimental configuration and beam conditions. This latter procedure, in particular, argues for the presence of structures for $^{12}C + ^{24}Mg$, and also for the observation of ≈ 100 mb difference in the σ_{fus}^{max} for the two systems.

Having established the presence of structures in the yields defined as evaporation residue, there is still the question of what uncertainties exist in the identification. A possible source of error is inclusion of small yields from other reactions, known to

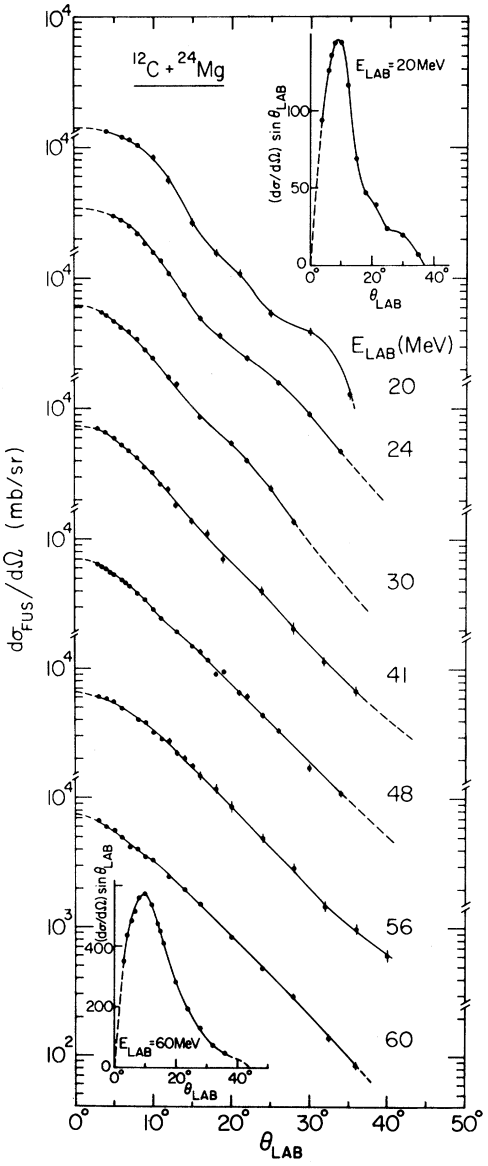

FIG. 4. Angular distribution of the fusion cross sections observed at various energies for the $^{12}C + ^{24}Mg$ system. At upper right and lower left are plots of $(d\sigma_{fus}/d\Omega)*\sin\theta_{lab}$ for the lowest and highest bombarding energies.

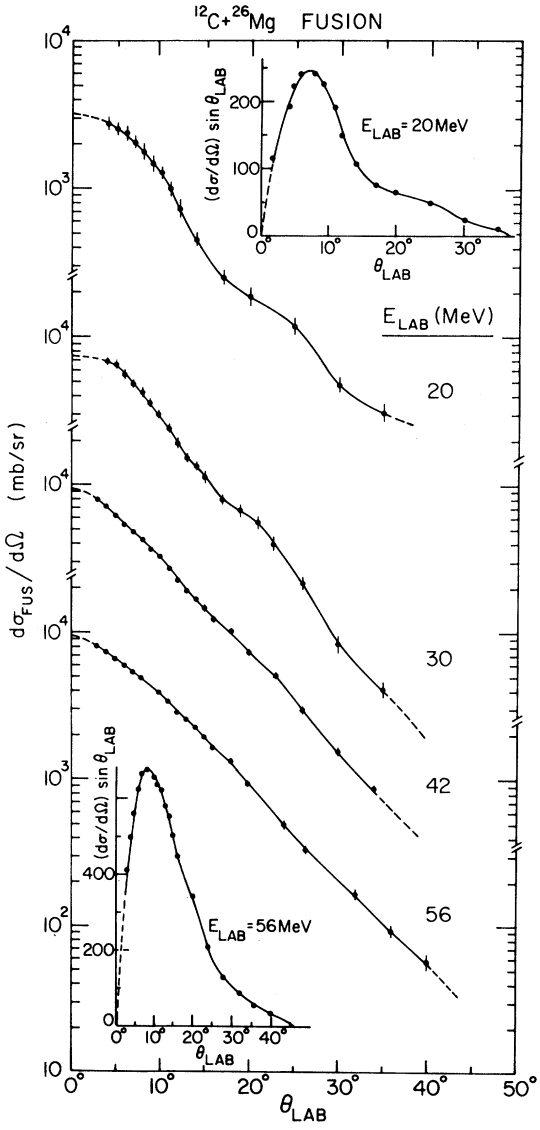

FIG. 5. Angular distribution of the fusion cross sections observed at various energies for the $^{12}C + ^{26}Mg$ system. At upper right and lower left are plots of $(d\sigma_{fus}/d\Omega)*\sin\theta_{lab}$ for the lowest and highest bombarding energies.

show structures in their excitation function. Potential reactions for such misidentification are $^{12}C + ^{12}C$ and $^{12}C + ^{16}O$, where both ^{12}C and ^{16}O are possible target contaminants. As discussed previously, efforts were made to minimize target oxidation and carbon buildup. The measurements show that fusion products from the above two reactions contribute negligible yields in the ΔE-E region of the $^{12}C + ^{24}Mg$ evaporation residues and are hence not responsible for the structures observed. Other potential sources of such yields are those resulting from other $^{12}C + ^{24}Mg$ exit channels. At question is whether, for example, the heavy recoils resulting from back angle elastic and inelastic scattering of ^{12}C (which are known to shown structures in their excitation function[8,17]) fall into the ΔE-E region identified as evaporation residue yields. Recent measurements for the $^{12}C + ^{20}Ne$ (Ref. 18) and $^{16}O + ^{27}Al$ (Ref. 19) systems indicate that at higher energies such processes may become

TABLE III. The total fusion cross section for $^{12}C + ^{24}Mg$. These cross sections are determined by integrating the area under the angular distribution for the fusion products. These results are compared to the total reaction cross sections which are established by optical model fits to elastic scattering.

E_{lab} (MeV)	σ_{fus} (mb)	σ^{om}_{react} (mb)
20.0	253±16	334
24.0	489±32	641
30.0	795±42	937
41.0	1050±55	1232
48.0	1100±63	1340
56.0	1161±65	1425
60.0	1180±78	1457

significant. In the energy region of the present study such processes are expected to be small, and, in fact, no evidence for such processes can be seen in those energy regions in ΔE-E space where they would be clearly resolved from the evaporation residues. Our observations are consistent with the finding of Novotny *et al.*[20] who, in an investigation of binary processes in the $^{12}C + ^{24}Mg$ reaction, found angular distribution behaviors that imply a small cross section for heavy recoils in the angular region of our measurements.

Further evidence that the structure observed is present in the fusion cross section comes from γ-ray measurements of Freeman *et al.*,[11] who find structures present in the excitation functions for yields associated with transitions in ^{31}P and ^{28}Si; nuclei interpreted as resulting from (αp) and (2α) evaporation of the compound nucleus, ^{36}Ar. In the energy range studied (i.e., $15 \lesssim E_{c.m.} < 23.7$ MeV), structures with maxima located at $E_{c.m.} \approx 20$ and 22.5

TABLE IV. The total fusion cross section for $^{12}C + ^{26}Mg$. These cross sections are determined by integrating the area under the angular distribution for the fusion products. These results are compared to the total reaction cross sections which are established by optical model fits to the elastic scattering.

E_{lab} (MeV)	σ_{fus} (mb)	σ^{om}_{react} (mb)
20.0	384±25	506
30.0	947±47	982
42.0	1132±68	1309
56.0	1280±70	1452

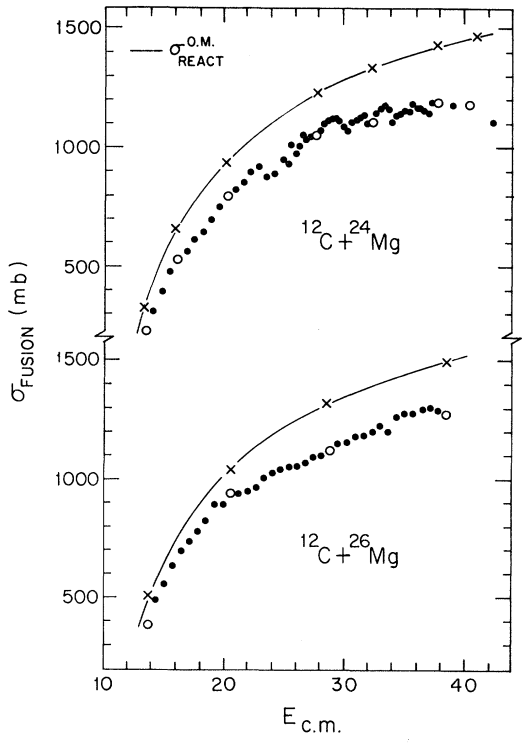

FIG. 6. Total fusion cross sections for $^{12}C + ^{24}Mg$ and $^{12}C + ^{26}Mg$ are plotted as a function of center of mass energy. The solid dots are the results of single angle measurement. The open circles are determined from full angular distributions. The solid curves are the optical model predictions of total reaction cross section.

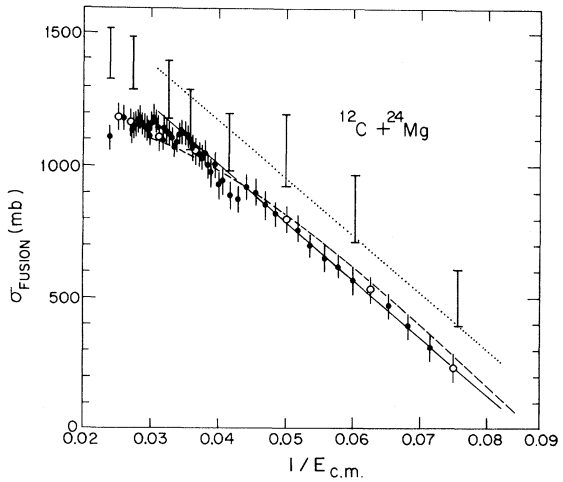

FIG. 7. The total fusion cross sections for $^{12}C + ^{24}Mg$ are shown plotted as a function of $1/E_{c.m.}$. The solid curve is a fit of the expression $\sigma(E) = \pi R_B^2(1 - V_B/E_{c.m.})$ to the low energy data (see text). The dashed curve is the prediction of the Bass model, and the dotted line has been hand drawn through the TDHF calculated cross section values.

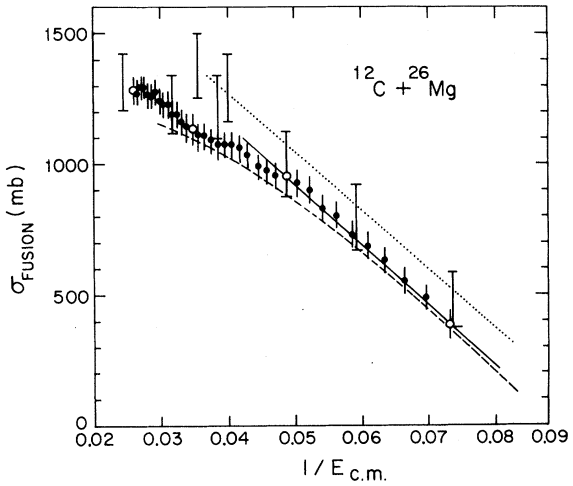

FIG. 8. The total fusion cross sections for $^{12}C + ^{26}Mg$ are shown plotted as a function of $1/E_{c.m.}$ The solid curve is a fit of the expression $\sigma(E) = \pi R_B 2(1 - V_B/E_{c.m.})$ to the energy data (see text). The dashed curve is the prediction of the Bass model, and the dotted line has been hand drawn through the TDHF calculated cross section values.

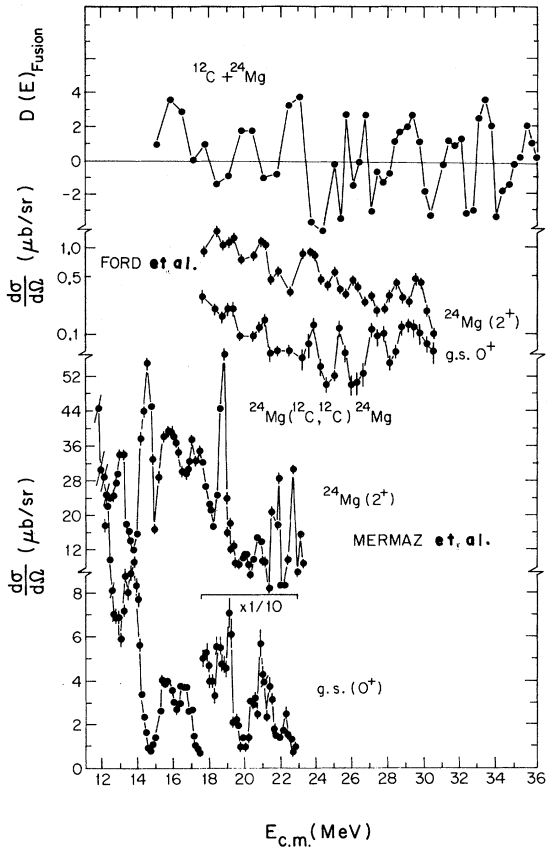

FIG. 9. The deviation function for the total fusion cross section of $^{12}C + ^{24}Mg$ is compared with the elastic and inelastic back angle scattering excitation functions of Refs. 17 and 24.

MeV were observed which are consistent with those observed in the present charged-particle measurements (see Fig. 9). In addition, γ-ray measurements performed at Argonne[21] show that structures continue to be present in the excitation functions at higher energies and that these structures are in reasonable agreement with those that have been seen in the charged-particle measurements. These considerations lead us to conclude that the structures observed in the present measurements are, in fact, associated with the fusion cross sections.

The observation of structures for the $^{12}C + ^{24}Mg$ systems and not for the $^{12}C + ^{26}Mg$ systems, of gross structures of widths ~ 2 MeV, and of structures in the α-evaporating channels[11,21] are very similar to those observed for the lighter systems involving C and O isotopes.[1,4] In the case of these latter systems, prominent structures in the fusion cross sections are observed for systems involving α nuclei (i.e., $^{12}C + ^{12}C$, $^{12}C + ^{16}O$, and $^{16}O + ^{16}O$), but not for others. For the identical systems, $^{12}C + ^{12}C$ and $^{16} + ^{16}O$, the spacing of the gross structures is consistent with the spacing of consecutive grazing (even) partial waves supporting the interpretation that the structures are associated with shape resonances of the ion-ion potential.[1,2] For $^{12}C + ^{16}O$, however, the observed spacings are still those expected in identical particle systems (i.e., where only the even partial waves can contribute), and hence is difficult to understand in terms of simple shape resonances. Further evidence for a more complicated mechanism for $^{12}C + ^{16}O$ comes from the observed fragmentation of the gross structures into sharper structures which show lack of correlation between the various channels.[22] In the present case of $^{12}C + ^{24}Mg$, the structure is not impressively periodic over the energy range studied. At lower energies the structures appear to be spaced roughly at every second grazing partial wave, while at higher energies the structures appear to be roughly at consecutive grazing waves. In regard to the question of whether the gross structure is fragmented, the present data are insufficient to allow one to draw any conclusions. A display of the deviation function for $^{12}C + ^{24}Mg$ fusion using the following relation,

$$D(E) = \frac{\sigma(E)}{\langle \sigma(E) \rangle} - 1 , \qquad (1)$$

where $\langle\sigma(E)\rangle$ is averaged over 4 MeV laboratory energy, is shown in Fig. 9. In this figure one can observe more clearly the presence of structures at lower energies, and the overall character of spacings and widths.

Other reaction channels for $^{12}C+^{24}Mg$ have been investigated and evidence for structures reported. Notably, Cindro *et al.*[23] have reported measurements for the $^{24}Mg(^{12}C,\alpha)^{32}S$ (g.s., 2^+) reactions over the energy range $27.5 \leq E_{lab} \leq 35.5$ MeV, and Ford *et al.*[24] and Mermaz *et al.*[17] have reported results of investigations of elastic and inelastic scattering at back angles. While a more detailed discussion of the comparison of structure in direct and fusion channels will be made in our γ-ray publication,[21] several interesting features can be noted here. In Fig. 9 the elastic and inelastic scattering excitation functions of Mermaz *et al.*[17] and Ford *et al.*[24] are compared with that observed in the fusion yields. The elastic and inelastic cross sections[17] show definite evidence of narrow intermediate structures of width $\lesssim 500$ keV which, if present in the fusion cross section, could account for the character of the structures observed. A second observation is that there is no obvious correlation between the structure in the fusion and that in the elastic and inelastic scattering functions. A final comment is that additional fine energy step elastic and inelastic scattering excitation functions, such as those of Mermaz at higher bombarding energy, would be of great interest. At $E_{c.m.} \simeq 24$ MeV the final cross section behavior appears to qualitatively change in character both in terms of the structure observed and in the average cross section behavior (as will be discussed in the next subsection). A comparison with direct channel behavior in this energy region would perhaps provide some insight into the nature of these phenomena.

B. Average cross section behavior

The general features of the fusion cross section behavior in the energy range under consideration here (i.e., from ~ 1 to 2.5 times the Coulomb barrier energy) have been well established in numerous measurements performed over the last few years.[3,9] As a function of bombarding energy the fusion cross section increases roughly linearly versus $1/E_{c.m.}$ until reaching a maximum, σ_{fus}^{max}, and then remains basically constant. This behavior for $^{12}C+^{24}Mg$ and $^{12}C+^{26}Mg$ can be seen in Figs. 6–8, where the fusion cross section for both systems reach maximum at $E_{c.m.} \approx 34$ MeV. In Fig. 6 the fusion cross sections are plotted versus $E_{c.m.}$ and the total reaction cross sections as obtained from optical model fits to the elastic scattering are indicated by solid lines. In these plots one can see that the distribution of reaction strength for the two systems differs significantly. It is interesting to note that for the $^{12}C+^{26}Mg$ system, for which no structure is observed, the fusion cross sections account for a greater fraction of the total reaction strength. It is also interesting to note that there is an apparent change in the slope of the fusion excitation function for $^{12}C+^{26}Mg$ at $E_{c.m.} \approx 22$ MeV. This is better observed in Fig. 8 where the deviation of the fusion cross section from a linear $1/E_{c.m.}$ behavior, as indicated by the solid lines, can be seen.

Such a $1/E_{c.m.}$ cross section behavior is expected in the phenomenological model of Glas and Mosel[25] in which it is assumed that the colliding ions must reach a certain critical distance before fusion occurs. At energies near and above the Coulomb barrier the behavior of the fusion cross section is dominated by the interaction barrier which must be surpassed in order to come into contact, and is predicted, in the classical limit to have the energy dependence,

$$\sigma_{fus}(E)=\pi R_B^2\left[1-\frac{V_B}{E_{c.m.}}\right], \tag{2}$$

where R_B and V_B are the barrier radius and height, respectively. Previous studies have shown that the fusion cross section behavior for other systems in this mass range can be well represented using Eq. (2),[3] and that there apparently exists an isotopic effect for systems involving different isotopes of the same element (i.e., the cross section at any specific $E_{c.m.}$ is larger for the larger or more massive isotope).[12,26] The solid lines shown in Figs. 7 and 8 are fits to the low energy data ($E_{c.m.} < 22$ MeV) by Eq. (2) and correspond to values of $R_B = 7.73$ fm and $V_B = 11.62$ MeV for the $^{12}C+^{24}Mg$ system, and $R_B = 8.14$ fm and $V_B = 11.10$ MeV for the $^{12}C+^{26}Mg$ system. These parameters reflect the observation of almost identical slopes for the two systems, but with ≈ 100 mb larger magnitude for $^{12}C+^{26}Mg$. This magnitude, indicated by the difference in R_B cannot be understood as arising only from a size difference. If one assumes $R_B \approx (A_1^{1/3}+A_2^{1/3})$ then one would expect an $\approx 1.5\%$ difference as opposed to the 5.3% effect observed in the extracted radii. (Electron scattering results[27] in fact indicate that the charge radii of ^{24}Mg and ^{26}Mg differ by only $\approx 0.5\%$.) Hence, while an "isotopic

effect" is expected, the magnitude appears to be larger than can be easily understood in the present treatment. Nor, as noted previously, can the observation of the departure from a $1/E_{\text{c.m.}}$ behavior at such a low bombarding energy for $^{12}C + ^{26}Mg$ be easily understood.

For a more realistic treatment of fusion, one must choose some nuclear potential in order to better describe the properties of the interaction barrier. Studies involving various types of potentials have been reported.[9,28,29] In general, these macroscopic models are unable to reproduce differences such as noted for the present system. Shown in Figs. 7 and 8 as dashed curves are the predictions of the Bass model[28] which utilizes an empirical potential established by fitting the fusion cross section behaviors for a number of systems. It is interesting to note that while the differences in magnitude are not reproduced (i.e., the prediction overestimates the cross section for $^{12}C + ^{24}Mg$ and underestimates that for $^{12}C + ^{26}Mg$), the observed departure from a $1/E_{\text{c.m.}}$ behavior for $^{12}C + ^{26}Mg$ does appear to be predicted. In this case it is $^{12}C + ^{24}Mg$ which displays a $1/E_{\text{c.m.}}$ behavior to a much higher energy that is at greater variance with the predicted trend, even though there appears to be a better fit to the data.

Finally, we have obtained theoretical values for the fusion cross sections by performing fully microscopic, time-dependent Hartree-Fock (TDHF) calculations. The calculations have been effected in the two-dimensional, axially symmetric, rigid clutching approximation,[30] and have utilized the finite range, nonlocal Skyrme potential *SII*, as described in Ref. 31, with a residual pairing interaction included within the constant G model.[32] The initial target and projectile wave functions have been calculated using the imaginary time step method.[33] The value $G=0.64$ MeV has been used for the constant strength of the pairing interaction for neutrons and for protons, in both the static calculations of the initial wave functions, and in subsequent dynamical calculations.

The calculated binding energies and rms radii for the projectile and for the target nuclei are compared with the values derived from experiment in Table V. Also given are the ratios of the calculated values of the electric quadrupole moment, $Q^e_{20}=\langle 2z^2-x^2-y^2\rangle_{\text{protons}}$, to Zr_{rms}^2. As indicated in the table, the binding energies are reproduced rather well, with the carbon projectile and magnesium targets underbound by but 6.3%, 3.4%, and 1%, respectively. The charge radii of the magnesium isotopes are equally well reproduced, in that they exceed the experimental values of the radii by but 2.3% and 3.6%, respectively. The charge radius of the carbon nucleus, however, exceeds the experimental value by 8.5%. Nevertheless, the ^{12}C wave function is significantly improved as compared to a previous version, calculated[37] using the filling approximation and a local version of the Skyrme potential. The last column of Table V in which values of the ratio $Q_{20}{}^2/Zr_{\text{rms}}2$ are listed, indicates that all of the calculated densities exhibit well established deformations.[38] As we shall discuss below, the interpretation of the fusion cross sections is complicated by the presence of the deformations.

The calculated $^{12}C + ^{24}Mg$ and $^{12}C + ^{26}Mg$ fusion cross sections are compared with the experimentally derived cross sections in Figs. 7 and 8. The cross sections have been calculated in the sharp cutoff approximation,[39] which has been fully discussed in Ref. 40. The uncertainties in the calculated cross sections are due entirely to uncertainties in the determination of the values of angular momentum for which the nuclei fuse. These uncertainties may be made arbitrarily small by performing additional calculations. However, we have here chosen to determine the values of angular momentum for which fusion occurs at a given energy only within two units of $\hbar$. The TDHF cross sections are plotted versus $1/E_{\text{c.m.}}$ in Figs. 7 and 8, and, as may be

TABLE V. Static properties of the HF densities of the projectile and target nuclei.

Nucleus	Binding energy (MeV) Th	Exp[a]	r_{rms} (fm) Th	Exp	$Q^e_{20}/Zr_{\text{rms}}{}^2$ Th
^{12}C	86.4	92.2	2.67	2.46[b]	−0.47
^{24}Mg	191.6	198.3	3.15	3.08[c]	0.56
^{26}Mg	214.6	216.7	3.17	3.06[c]	0.58

[a]Reference 34.
[b]Reference 35.
[c]Reference 36.

observed, are fairly well fitted by straight lines of the same slope as the experimental cross sections. Although the TDHF cross sections are consistently too high, they scale with the experimental cross sections in that the $^{12}C + ^{26}Mg$ cross section exceeds that for the $^{12}C + ^{24}Mg$ reaction by some 100 mb. As noted in the discussion of the macroscopic models, this difference in cross section is attributable to dynamic rather than geometric effects. Indeed, referring to the data in Table V, we note that there is but a $\frac{1}{2}\%$ difference in the charge radii of ^{24}Mg and ^{26}Mg, with the experimental radius of ^{24}Mg in fact exceeding that of ^{26}Mg. In addition, the calculated value of the ^{26}Mg neutron radius exceeds that of the ^{24}Mg neutron radius by only 3.5%. Thus, on the basis of geometry alone, one would expect the difference in cross sections to be on the order of $2\times 3.5\% = 7\%$, whereas the experimental cross sections differ by approximately 25% at the lowest energies studied.

That the resonant structure exhibited by the $^{12}C + ^{24}Mg$ fusion cross section is not reproduced by the TDHF calculation is not surprising. As previously discussed, the resonant structure may be traced to the alpha evaporation channels, and the TDHF calculations which, at best, reproduce the average behavior of the system, are not expected to fit structure due to specific exit channels. Both in the present calculations, and in calculations[37] of the system $^{12}C + ^{16}O$, the TDHF cross section is a smooth function of the energy.

It is tempting to ascribe the gross difference in the TDHF and experimental cross sections to the inadequacies of the ^{12}C wave function, which gives a charge radius 8.5% larger than the measured value. Indeed, on the basis of geometry, this error leads to 17% overestimation of the cross section (approximately 150 mb at $E_{\text{c.m.}} = 20$ MeV). However, the cross sections plotted have been calculated for the case of oblate ^{12}C projectiles incident upon $^{24,26}Mg$ targets, which are prolate about the same axis of symmetry. Since the density overlap, and hence the energy of the interaction, depend[41] upon the relative orientation of the nuclei, the cross section should be obtained by averaging over relative orientation. Although we have not effected such an average, we have calculated the cross sections for *prolate* ^{12}C projectiles incident upon Mg targets, which, as before, are prolate about the same axis of symmetry. The impact of this change is to uniformly increase the calculated cross section by approximately 350 mb. While this certainly is a dramatic increase, it should be noted that the prolate ^{12}C wave function is extremely poor, and gives rise to a nuclear binding energy of but 74 MeV, a value more than 12 MeV less than that of the oblate solution, and over 18 MeV less than the experimental binding. Thus, for averaging purposes it would have been far superior to rotate the oblate ^{12}C wave function on the mesh, rather than effecting the present calculation, which more or less represents a collison between a highly excited ^{12}C nucleus and Mg. Nevertheless, the large effect suggest that even with a more compact ^{12}C wave function, suitable averaging of the cross section will result in a fusion cross section larger than found experimentally.

In the case of the $^{12}C + ^{26}Mg$ reaction, the saturation of the fusion cross section at high energy appears to be reproduced well by the TDHF calculation. The saturation may be understood in terms of the liquid drop model by stating that there exists a maximum angular momentum which the compound nucleus formed in the reaction can sustain without breaking apart. Once this angular momentum has been realized, the cross section can then only decrease as the bombarding energy is increased, due to the kinematical factor $1/E_{\text{c.m.}}$ in the cross section. At the highest energies studied, the TDHF calculations result in fusion for angular momenta less than or equal to $25\hbar$ for an oblate ^{12}C incident upon a prolate Mg target, and less than or equal to $30\hbar$ for a prolate ^{12}C projectile incident upon a prolate Mg target. We simply note that these values of the saturation value of the angular momentum are not in disagreement with the liquid drop limit[42] of approximately $30\hbar$ for the compound nucleus ^{36}Ar.

Returning to the results of the experiment, the present data indicate that the $^{12}C + ^{24}Mg$ and $^{12}C + ^{26}Mg$ systems have $\sigma_{\text{fus}}^{\max}$ of 1160 ± 50 mb, and 1280 ± 70 mb, respectively. Variations of this magnitude for this range have been reported previously[3,6] and shown in Fig. 10 are results for ^{12}C and ^{16}O projectiles on various *sd*-shell nuclei.[1,12–14,43–47] All the systems shown have $\sigma_{\text{fus}}^{\max}$ of ≈ 1200 mb, with exception of $^{12}C + ^{28}Si$ with $\sigma_{\text{fus}}^{\max} \approx 1000$ mb. In the case of $^{16}O + ^{28}Si$, two values of $\sigma_{\text{fus}}^{\max}$ are reported; $\sigma_{\text{fus}}^{\max} \simeq 1050$ mb (Ref. 12) and 1200 mb.[46] Comparison of the present measurements to those for $^{16}O + ^{24}Mg$ and $^{16}O + ^{26}Mg$ (Ref. 13) shows that for both projectiles the ^{26}Mg nucleus is associated with ≈ 100 mb larger $\sigma_{\text{fus}}^{\max}$ than that of the ^{24}Mg nucleus, and that for both Mg isotopes the reactions involving ^{12}C have $\sigma_{\text{fus}}^{\max}$ that are somewhat larger than those associated with ^{16}O. In the case of the differences observed for

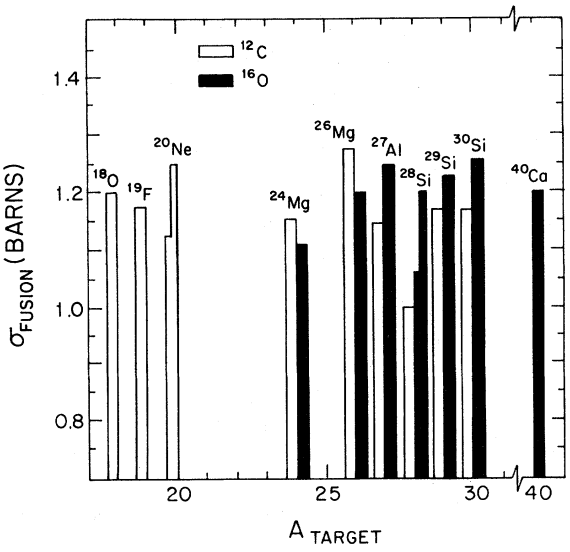

FIG. 10. Comparison of σ_{fus}^{max} observed for ^{12}C and ^{16}O projectiles on various *sd*-shell nuclei. The values are from the present study and Refs. 1, 12–14, and 43–48. The half bar indicates two measurements for the same reaction which differ significantly.

^{24}Mg and ^{26}Mg, the direction and magnitudes of the differences are roughly consistent with those predicted by entrance channel models. In the case of the differences observed for systems involving ^{12}C and ^{16}O, the present results are anomalous in that for the other systems studied (e.g., ^{12}C and ^{16}O on ^{27}Al and $^{28-30}$Si), the systems involving ^{16}O are observed to have larger σ_{fus}^{max}.

V. SUMMARY AND CONCLUSION

In the present study the total fusion cross sections for the $^{12}C + ^{24}Mg$ and $^{12}C + ^{26}Mg$ systems have been established by measurements of evaporation residues. The fusion cross section excitation function for $^{12}C + ^{24}Mg$ is found to exhibit structures with peak-to-valley variation of 5–10%, while that for $^{12}C + ^{26}Mg$ behaves relatively smoothly. The structures observed in the present measurement are consistent with those reported in γ-ray studies in the energy range in which there is overlap. Comparison with the excitation function for elastic and inelastic scattering at back angles shows that the structures observed are qualitatively similar, but no firm evidence for correlations is noted. Comparison of the average fusion cross section behavior for the $^{12}C + ^{24}Mg$ and $^{12}C + ^{26}Mg$ systems reveals similar $1/E_{c.m.}$ energy dependence at the lower energies ($E_{c.m.} \leq 22$ MeV) and an ≈ 100 mb larger magnitude for the $^{12}C + ^{26}Mg$ system. At higher energies the $^{12}C + ^{26}Mg$ system shows evidence for anomalous departure from the $1/E_{c.m.}$ behavior at an energy significantly lower than where the cross section is observed to saturate. The observed σ_{fus}^{max} for $^{12}C + ^{26}Mg$ is ≈ 100 mb larger than that observed for $^{12}C + ^{24}Mg$, and the σ_{fus}^{max} associated with $^{12}C + ^{24}Mg(^{26}Mg)$ is larger than that for $^{16}O + ^{24}Mg(^{26}Mg)$. These differences cannot be easily understood in the framework of the models discussed.

ACKNOWLEDGMENTS

We wish to thank Mr. G. Thomas for preparing the targets. This research was supported by the U. S. Department of Energy under Contract W-31-109-Eng-38, under Contract W-7405-Eng-26 with the Union Carbide Corporation, and by the National Science Foundation (Grant No. NSF 77-12879).

*Present address: Physics Department, Auburn University, Auburn University, Alabama 36849.

[1]P. Sperr, S. E. Vigdor, Y. Eisen, W. Henning, D. G. Kovar, T. R. Ophel, and B. Zeidman, Phys. Rev. Lett. 36, 405 (1976); P. Sperr, T. H. Braid, Y. Eisen, D. G. Kovar, F. W. Prosser, Jr., J. P. Schiffer, S. L. Tabor, and S. E. Vigdor, *ibid.* 37, 321 (1976).

[2]J. J. Kolata, R. M. Freeman, F. Haas, B. Heusch, and A. Gallmann, Phys. Lett. 65B, 333 (1976); J. J. Kolata, R. C. Fuller, R. M. Freeman, F. Haas, B. Heusch, and A. Gallmann, Phys. Rev. C 16, 891 (1977); 19, 2237 (1979).

[3]D. G. Kovar, D. F. Geesaman, T. H. Braid, Y. Eisen, W. Henning, T. R. Ophel, M. Paul, K. E. Rehm, S. J. Sanders, P. Sperr, J. P. Schiffer, S. L. Tabor, S. Vigdor, and B. Zeidman, Phys. Rev. C 20, 1305 (1979).

[4]D. G. Kovar, *Lecture Notes in Physics No. 92: Nuclear Interaction,* edited by B. A. Robson (Springer, Berlin, 1979), p. 329.

[5]J. P. Wieleczko, S. Farrar, M. Conjeaud, and F. Saint-Laurent, Phys. Lett. 9313, 35 (1980).

[6]D. Konnerth, K. G. Bernhardt, K. A. Eberhard, R. Singh, A. Strazalkowski, W. Trautman, and W. Trombik, Phys. Rev. Lett. 45, 1154 (1980).

[7]J. Barrette, M. J. Levine, P. Braun-Munzinger, G. M. Berkowitz, M. Gai, J. W. Harris, and C. M. Jachcinski, Phys. Lett. 40, 445 (1978); J. Barrette *et al.*, Phys. Rev. C 20, 1959 (1979).

[8]M. R. Clover, R. M. DeVries, R. Ost, N. J. A. Rust, R. N. Cherry, Jr., and H. E. Gove, Phys. Rev. Lett. 40, 1008 (1978).

[9]J. R. Birkelund, L. E. Tubbs, J. R. Huizenga, J. N. De, and D. Sperber, Phys. Rep. 56, 107 (1979).

[10]P. Deyoung, J. Kolata, R. Malmin, S. Tripathi, R. Luhn, and S. Davis, Bull. Am. Phys. Soc. 24, 851 (1979).

[11]R. M. Freeman, F. Haas, B. Heusch, and S. M. Lee, Phys. Rev. C 20, 569 (1979).

[12]W. J. Jordan, J. V. Maher, and J. C. Peng, Phys. Lett. 87B, 38 (1979).

[13]S. L. Tabor, D. F. Geesaman, W. Henning, D. G. Kovar, K. E. Rehm, and F. W. Prosser, Jr., Phys. Rev. C 17, 2136 (1978).

[14]D. F. Geesaman, C. N. Davids, W. Henning, D. G. Kovar, K. E. Rehm, J. P. Schiffer, S. L. Tabor, and F. W. Prosser, Jr., Phys. Rev. C 18, 284 (1978).

[15]M. M. Fowler and R. C. Jared, Nucl. Instrum. Methods 124, 341 (1975).

[16]D. H. Gloeckner, M. H. MacFarlane, and S. C. Pieper, Argonne National Laboratory Informal Report No. ANL-76-11, 1978 (unpublished).

[17]M. C. Mermaz, A. Greiner, B. T. Kim, M. J. LeVine, E. Müller, M. Ruscev, M. Petrascu, M. Petrovivi, and V. Simon, Phys. Rev. C 24, 1512 (1981).

[18]D. Shapira, J. L. C. Ford, Jr., J. Gomez del Campo, R. G. Stokstad, and R. M. DeVries, Phys. Rev. Lett. 43, 1781 (1979).

[19]D. Shapira, J. L. C. Ford, Jr., J. Gomez del Campo, and P. H. Stelson, Phys. Rev. C 21, 1824 (1980).

[20]R. Novotny, G. Hammer, D. Pelte, H. Emling, and D. Schwalm, Nucl. Phys. A294, 255 (1978).

[21]K. Daneshvar, D. G. Kovar, and C. N. Davids, Bull. Am. Phys. Soc. 24, 666 (1979); (unpublished).

[22]J. J. Kolata, R. M. Freeman, F. Haas, B. Heusch, and A. Gallmann, Phys. Rev. C 19, 408 (1979).

[23]N. Cindro, J. D. Moses, N. Stein, M. Cates, D. M. Drake, D. L. Hansen, and J. W. Sunier, Phys. Lett. 84B, 55 (1979).

[24]J. L. C. Ford, Jr., J. Gomez del Campo, D. Shapira, M. R. Clover, R. M. DeVries, B. R. Fulton, R. Ost, and C. M. Maguire, Phys. Lett. 89B, 48 (1979).

[25]D. Glas and U. Mosel, Nucl. Phys. A264, 268 (1976).

[26]Y. Eisen, J. Tserruya, Y. Eyal, Z. Fraenkel, and M. Hillman, Nucl. Phys. A291, 459 (1977).

[27]E. W. Lees, C. S. Carran, T. E. Drake, W. A. Gillespie, A. Johnston, and R. P. Singhal, J. Phys. G 2, 105 (1976).

[28]R. Bass, Phys. Rev. Lett. 39, 265 (1977).

[29]H. Krappe, J. R. Nix, and A. J. Sierk, Phys. Rev. C 20, 992 (1979).

[30]S. E. Koonin, K. T. R. Davies, V. Maruhn-Rezwani, H. Feldmeier, S. J. Krieger, and J. W. Negele, Phys. Rev. C 15, 1359 (1977).

[31]J. W. Negele, S. E. Koonin, P. Möller, J. R. Nix, and A. J. Sierk, Phys. Rev. C 17, 1098 (1978).

[32]J. Blocki and H. Flocard, Nucl. Phys. A273, 45 (1976).

[33]K. T. R. Davies, H. Flocard, S. J. Krieger, and M. S. Weiss, Nucl. Phys. A342, 111 (1980).

[34]A. H. Wapstra and K. Bos, At. Data Nucl. Data Tables 19, 175 (1977).

[35]G. Fey, H. Frank, W. Shütz, and H. Theissen, Z. Phys. 265, 401 (1973).

[36]E. W. Lees, C. S. Curran, T. E. Drake, W. A. Gillespie, A. Johnston, and R. P. Singhal, J. Phys. G 2, 105 (1976).

[37]S. J. Krieger and K. T. R. Davies, Phys. Rev. C 20, 167 (1979).

[38]A determinental wave function for the prototypical deformed *sd*-shell nucleus ^{20}Ne yields the value $Q^e_{20}/\mathrm{Zr}_{\mathrm{rms}}^2 \simeq 0.6$.

[39]P. Bonche, B. Grammaticos, and S. E. Koonin, Phys. Rev. C 17, 1700 (1978).

[40]S. J. Krieger and K. T. R. Davies, Phys. Rev. C 18, 2567 (1978).

[41]M. Arnould and W. M. Howard, Nucl. Phys. A274, 295 (1976).

[42]W. D. Myers and W. J. Swiatecki, Ann. Phys. (N.Y.) 55, 395 (1966).

[43]F. Saint-Laurent, M. Conjeaud, S. Harar, J. M. Loiseaux, J. Menel, and J. B. Viano, Nucl. Phys. A327, 517 (1979).

[44]J. Tserruya, J. Barrette, S. Kubono, P. Braun-Munzinger, M. Gai, and C. D. Uhlhorn, Phys. Rev. C 21, 1864 (1980).

[45]B. B. Back, R. R. Betts, C. Gaarde, J. S. Larsen, E. Michelsen, and Tai Kuang-Shi, Nucl. Phys. A285, 317 (1977).

[46]R. Rascher, W. F. J. Muller, and K. P. Lieb, Phys. Rev. C 20, 1028 (1979).

[47]S. E. Vigdor, D. G. Kovar, P. Sperr, J. Mahoney, A. Menchaca-Racha, C. Olmer, and M. S. Zisman, Phys. Rev. C 20, 2147 (1979).